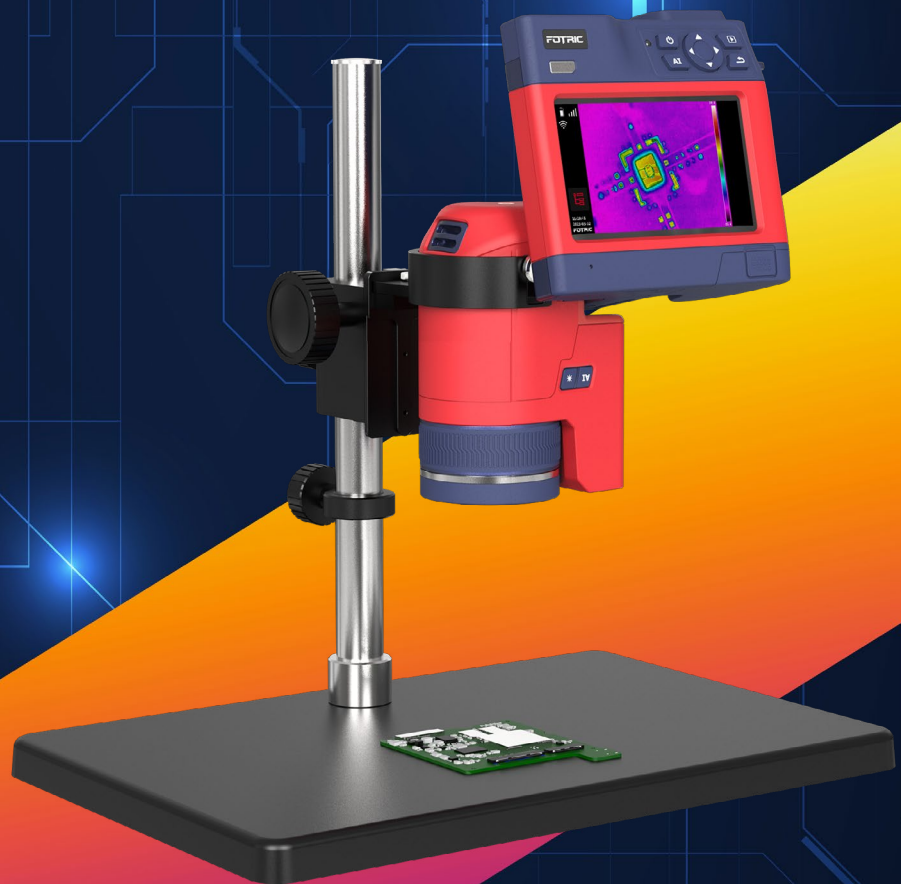


FOTRIC 220 Pro

Professional Handheld R&D Camera

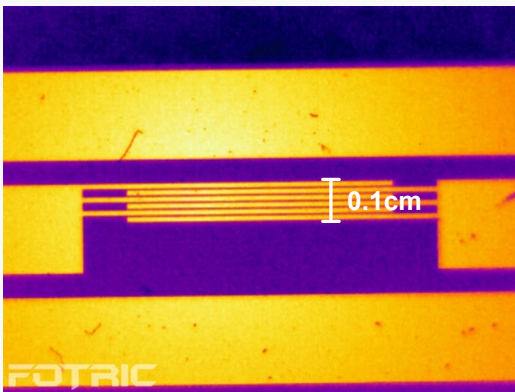
- > R&D in Universities and Research Institutes
- > Industrial Labs



Unlock Discovery with Unprecedented Clarity

> Up to 20 μ m Macro Lens

The FOTRIC macro lens boasts outstanding optical performance, effortlessly capturing clear images of extremely fine details and providing precise temperature distribution data.

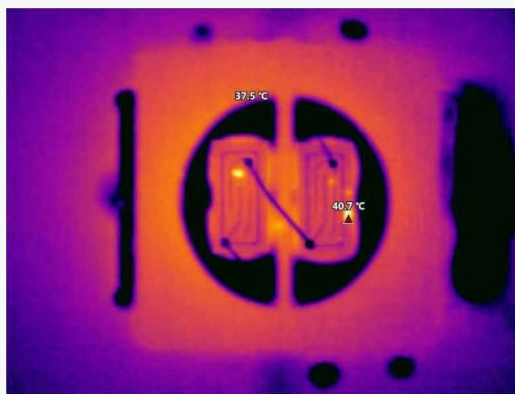


Electrode etching



Note:

Laser-etched electrical circuits are essential tools in MEMS. Thermal imaging simplifies the inspection of installation integrity across different substrate materials. When equipped with a macro lens, it also allows for a more detailed evaluation of circuit performance.



LED chip



Note:

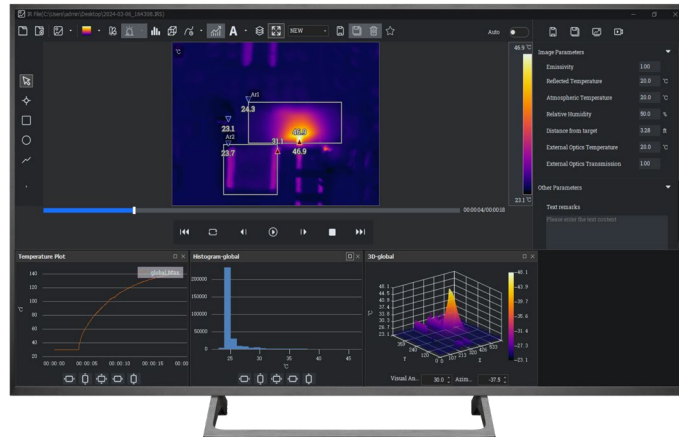
In microelectronics, thermal cameras play a crucial role in optimizing performance and design while ensuring product quality. By identifying heat generation points during operation, researchers can better understand thermal behavior and make necessary adjustments to improve efficiency and prevent overheating. This detailed thermal analysis aids in refining designs and addressing potential issues during the development process.

Unleash Your Video Data's Full Potential

> Radiometric Mastery

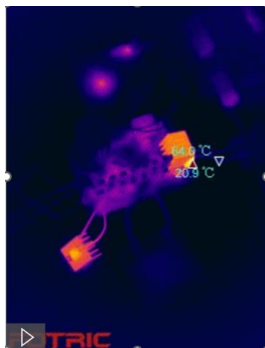
The AnalyzIR software supports dissecting your video data from every aspect.

- Time-temperature curve
- Distribution histogram
- 3D diagram

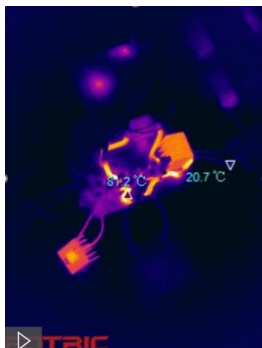


> Frame by Frame Analysis

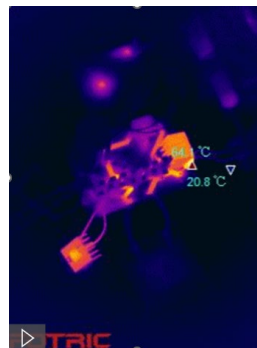
The fleeting moment when the rectifier bridge is pierced by the current.



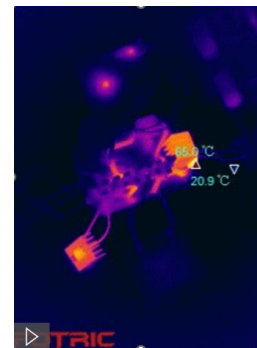
2min 2sec 291ms



2min 2sec 385ms



2min 2sec 525ms



2min 2sec 666ms

After analyzing frame by frame with AnalyzIR, it became evident that the sudden rise in temperature was caused by the current piercing the rectifier bridge, initially suspected to be an issue with the DSP (digital signal processor).

Unwaivering Commitment for Accuracy

Up to
1280x1024
IR Resolution

Up to
30mK
Thermal Sensitivity

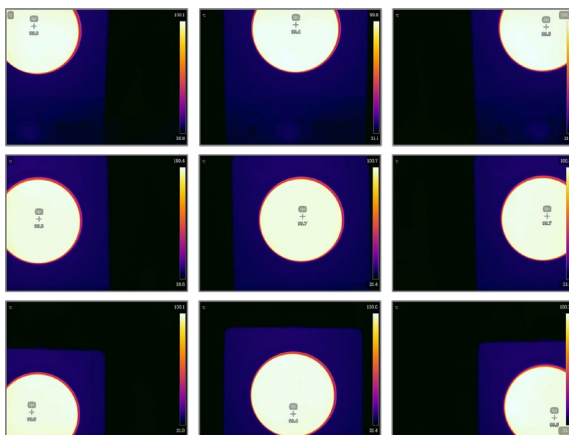
Up to
±1°C / 1%
Accuracy

> Exceptional Thermal Stability



After reaching thermal equilibrium, the camera's temperature fluctuation is less than 0.5°C.

> Extraordinary Temperature Uniformity



±0.4°C

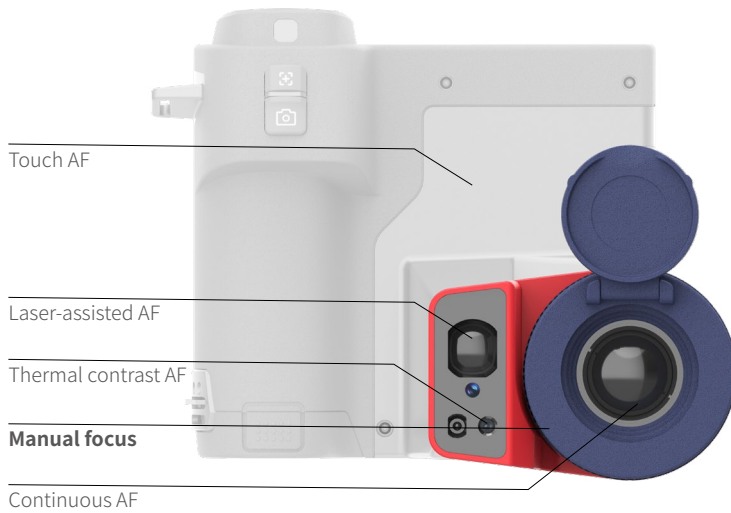
Margin of error against the center region

Note:

The thermal camera was aimed at a 100°C black body, measuring temperatures at the center, four corners, and along the edges of the screen. All nine points showed nearly identical results, demonstrating exceptional measurement uniformity.

Designed for User Experience

> TurboFocus® Intelligent Focus System



Instant Autofocus

Deliver fast and silent focus at mid and long range.

Precise Manual Focus

Enables fined-tuned observation at close distance.

> Professional Test Bench

Precision Meets Versatility

Elevate your testing with our advanced test bench, designed for precise adjustments and effortless maneuverability. Perfect for demanding R&D, industrial, or educational applications, it ensures seamless, accurate results every time.



Trusted by Researchers Across the Globe

► Publication List

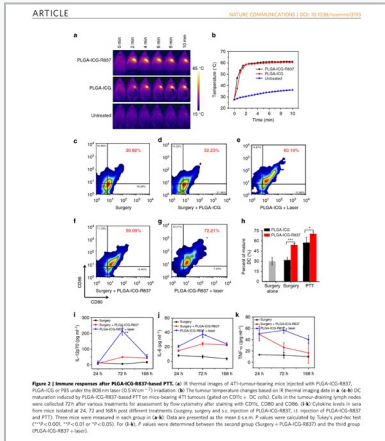


Figure 2 Immune response after PLGA-ICG-R837-based PDT. **a**, Normal images of 4T1 tumour-bearing mice injected with PLGA-ICG-R837, PLGA-ICG or PBS under the 808 nm laser. **b**, The tumour temperature changes before and after laser irradiation at 808 nm. **c**, The immune response induced by PLGA-ICG-R837-based PDT in mice bearing 4T1 tumours (group on CD45⁺ CD3⁺ cells). **d**, The immune response induced by PLGA-ICG-R837-based PDT in mice bearing 4T1 tumours (group on CD45⁺ CD8⁺ cells). **e**, The immune response induced by PLGA-ICG-R837-based PDT in mice bearing 4T1 tumours (group on CD45⁺ CD4⁺ cells). **f**, The immune response induced by PLGA-ICG-R837-based PDT in mice bearing 4T1 tumours (group on CD45⁺ CD8⁺ cells). **g**, The immune response induced by PLGA-ICG-R837-based PDT in mice bearing 4T1 tumours (group on CD45⁺ CD4⁺ cells). **h**, The immune response induced by PLGA-ICG-R837-based PDT in mice bearing 4T1 tumours (group on CD45⁺ CD8⁺ cells). **i**, The immune response induced by PLGA-ICG-R837-based PDT in mice bearing 4T1 tumours (group on CD45⁺ CD4⁺ cells). **j**, The immune response induced by PLGA-ICG-R837-based PDT in mice bearing 4T1 tumours (group on CD45⁺ CD8⁺ cells). **k**, The immune response induced by PLGA-ICG-R837-based PDT in mice bearing 4T1 tumours (group on CD45⁺ CD4⁺ cells). **l**, The immune response induced by PLGA-ICG-R837-based PDT in mice bearing 4T1 tumours (group on CD45⁺ CD8⁺ cells). **m**, The immune response induced by PLGA-ICG-R837-based PDT in mice bearing 4T1 tumours (group on CD45⁺ CD4⁺ cells). **n**, The immune response induced by PLGA-ICG-R837-based PDT in mice bearing 4T1 tumours (group on CD45⁺ CD8⁺ cells). **o**, The immune response induced by PLGA-ICG-R837-based PDT in mice bearing 4T1 tumours (group on CD45⁺ CD4⁺ cells). **p**, The immune response induced by PLGA-ICG-R837-based PDT in mice bearing 4T1 tumours (group on CD45⁺ CD8⁺ cells). **q**, The immune response induced by PLGA-ICG-R837-based PDT in mice bearing 4T1 tumours (group on CD45⁺ CD4⁺ cells). **r**, The immune response induced by PLGA-ICG-R837-based PDT in mice bearing 4T1 tumours (group on CD45⁺ CD8⁺ cells). **s**, The immune response induced by PLGA-ICG-R837-based PDT in mice bearing 4T1 tumours (group on CD45⁺ CD4⁺ cells). **t**, The immune response induced by PLGA-ICG-R837-based PDT in mice bearing 4T1 tumours (group on CD45⁺ CD8⁺ cells). **u**, The immune response induced by PLGA-ICG-R837-based PDT in mice bearing 4T1 tumours (group on CD45⁺ CD4⁺ cells). **v**, The immune response induced by PLGA-ICG-R837-based PDT in mice bearing 4T1 tumours (group on CD45⁺ CD8⁺ cells). **w**, The immune response induced by PLGA-ICG-R837-based PDT in mice bearing 4T1 tumours (group on CD45⁺ CD4⁺ cells). **x**, The immune response induced by PLGA-ICG-R837-based PDT in mice bearing 4T1 tumours (group on CD45⁺ CD8⁺ cells). **y**, The immune response induced by PLGA-ICG-R837-based PDT in mice bearing 4T1 tumours (group on CD45⁺ CD4⁺ cells). **z**, The immune response induced by PLGA-ICG-R837-based PDT in mice bearing 4T1 tumours (group on CD45⁺ CD8⁺ cells).

Article: «Photothermal therapy with immune-adjuvant nanoparticles together with checkpoint blockade for effective cancer immunotherapy»

Publication: «Nature»

Model: FOTRIC 225

mouse sera after found that mice of IL-12p70, those in sera of ementary Fig. 4). effect of PLGA-stained release of

Such results suggest that R837-containing nanoparticles could potentially act as an adjuvant to promote immunological responses of tumour-associate antigens in cell residues.

In our further *in vivo* experiment, BALB/c mice-bearing subcutaneous 4T1 tumours were intratumourally (i.t.) injected with PLGA-ICG or PLGA-ICG-R837 and then irradiated by an 808 nm laser at the power density of 0.5 W cm⁻² for 10 min. As monitored by an infrared thermal camera (Fotric 225), the tumour temperature of mice injected with PLGA-ICG or PLGA-ICG-R837 under laser irradiation quickly rose to ~60 °C, which was high enough to effectively ablate tumours

93 | www.nature.com/naturecommunications

3

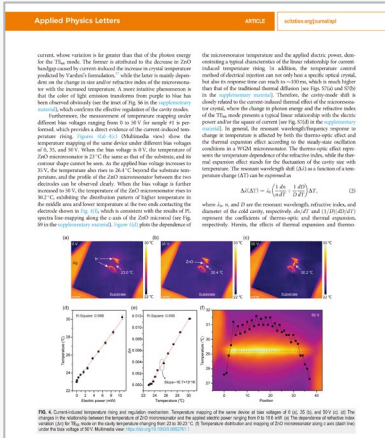


Fig. 4 Characterization and results for the APF resonator and optically active plasma. **a**, Schematic diagram of the experimental setup for generating the optical microresonator (APF) and performing transient measurements. **b**, SEM images of the resonator. **c**, The temperature profile on the resonator. **d**, The phase shift profile on the resonator. **e**, The relationship between the temperature and the phase shift. **f**, The relationship between the temperature and the phase shift. **g**, The relationship between the temperature and the phase shift. **h**, The relationship between the temperature and the phase shift. **i**, The relationship between the temperature and the phase shift. **j**, The relationship between the temperature and the phase shift. **k**, The relationship between the temperature and the phase shift. **l**, The relationship between the temperature and the phase shift. **m**, The relationship between the temperature and the phase shift. **n**, The relationship between the temperature and the phase shift. **o**, The relationship between the temperature and the phase shift. **p**, The relationship between the temperature and the phase shift. **q**, The relationship between the temperature and the phase shift. **r**, The relationship between the temperature and the phase shift. **s**, The relationship between the temperature and the phase shift. **t**, The relationship between the temperature and the phase shift. **u**, The relationship between the temperature and the phase shift. **v**, The relationship between the temperature and the phase shift. **w**, The relationship between the temperature and the phase shift. **x**, The relationship between the temperature and the phase shift. **y**, The relationship between the temperature and the phase shift. **z**, The relationship between the temperature and the phase shift.

Article: «Dynamic regulating of lasing mode in a whispering-gallery micro-resonator by thermo-optic effect»

Publication: «Applied Physics Letters»

Model: FOTRIC 228S

ation of the to develop of the cavity ve photonic

to the ZnO nductivity to rial) without see Fig. S1 in by electrical lasing mode fect and the to the resonance

0.03 nm) equipped with a CCD detector and the optically triggered streak camera (Optronix, Optoscope sc-10). The absorption spectrum is measured by a UV-Vis-NIR spectrophotometer (UV-3600 Plus, Shimadzu). The bias voltage is applied through a low-noise power supply equipment (Keysight, 2961A). The temperature mapping is presented by a thermal imager (FOTRIC, 228S-M20) equipped with an infrared magnifying lens with a resolution of 20 μm. The finite difference time domain (FDTD) method is performed to simulate the electric-field distribution of the fundamental mode confined in the optical microresonator with a resonant wavelength of 400 nm shown in Fig. S2. The structure model of microresonator has a diameter of 5 μm and a refractive index of 2.3.

93 | www.nature.com/naturecommunications

3

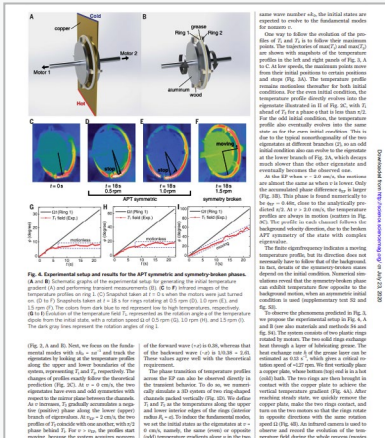


Fig. 5 Experimental setup and results for the APF resonator and optically active plasma. **a**, Schematic diagram of the experimental setup for generating the optical microresonator (APF) and performing transient measurements. **b**, SEM images of the resonator. **c**, The temperature profile on the resonator. **d**, The phase shift profile on the resonator. **e**, The relationship between the temperature and the phase shift. **f**, The relationship between the temperature and the phase shift. **g**, The relationship between the temperature and the phase shift. **h**, The relationship between the temperature and the phase shift. **i**, The relationship between the temperature and the phase shift. **j**, The relationship between the temperature and the phase shift. **k**, The relationship between the temperature and the phase shift. **l**, The relationship between the temperature and the phase shift. **m**, The relationship between the temperature and the phase shift. **n**, The relationship between the temperature and the phase shift. **o**, The relationship between the temperature and the phase shift. **p**, The relationship between the temperature and the phase shift. **q**, The relationship between the temperature and the phase shift. **r**, The relationship between the temperature and the phase shift. **s**, The relationship between the temperature and the phase shift. **t**, The relationship between the temperature and the phase shift. **u**, The relationship between the temperature and the phase shift. **v**, The relationship between the temperature and the phase shift. **w**, The relationship between the temperature and the phase shift. **x**, The relationship between the temperature and the phase shift. **y**, The relationship between the temperature and the phase shift. **z**, The relationship between the temperature and the phase shift.

Article: «Anti-parity-time symmetry in diffusive systems»

Publication: «Science»

Model: FOTRIC 233S

nd thickness around $d = 0.5$ mm. According to the derivation following Eq. (S. 1) the rotation speed $\dot{\theta}$ is $\dot{\theta} = \kappa_2 (\rho c)^{-1} (h d)^{-1} = 0.13$ s⁻¹. Therefore, the critical rotation speed $\dot{\theta}_c$ is $\dot{\theta}_c = \kappa_2 (\rho c R_1) = \dot{\theta} = 1.27$ rpm. To generate temperature gradient, the bottom of the copper plate was immersed in 70 °C hot water, while the top was covered by an ice bag. The temperature evolutions were measured with a Fotric 233s infrared camera, whose imaging resolution is 160 × 120 pixel and 0.1 °C, respectively.

Trusted by Researchers Across the Globe

> Publication List

Publication	Article	Model
Applied Thermal Engineering	Investigation on the microwave drying kinetics and pumping phenomenon of lignite spheres	FOTRIC 226
CARBON	Spray-freezing Induced Multidimensional Morphology Tuning of Assembled Spherical Carbon for Solar-driven Steam Generation	FOTRIC 260
Carbon	Fabrication of core-shell nanostructured poly(3,4-ethylenedioxythiophene)/carbon nanotube composites with enhanced thermoelectric power factor	FOTRIC 226
Science	Anti-Parity-Time Symmetry in Diffusive Systems	FOTRIC 224S
Journal of Food Engineering	Continuous flow microwave system with helical tubes for liquid food heating	FOTRIC 285
ACS Applied Nano Materials	Plasma Cleaning and Self-Limited Welding of Silver Nanowire Films for Flexible Transparent Conductors	FOTRIC 322Pro
Nano Today	Edge confined covalent organic framework with efficient biocompatibility and photothermic conversion	FOTRIC 345
Carbon	A structure evolution mechanism for the modulus loss in electromechanical response of carbon nanotube fiber	FOTRIC 615C
Applied Physics Letters	Dynamic regulating of lasing mode in a whispering-gallery microresonator by thermo-optic effect	FOTRIC 228S
Nature	Non-Hermitian topological whispering gallery	FOTRIC 228S
Foods	Efficient Solar-Driven Water Purification Based on Biochar with Multi-Level Pore Bundle Structure for Preparation of Drinking Water	FOTRIC 226S
Applied Materials Today	Stiffness tunable implanted electrode enabled by magnetic liquid metal for wireless hyperthermia	FOTRIC 228S
Nanomaterials	Design and Analysis of a Hollow Metallic Microlattice Active Cooling System for Microsatellites	FOTRIC 618C
Applied Thermal Engineering	Thermal management of 3D chip with non-uniform hotspots by integrated gradient distribution annular-cavity micro-pin fins	FOTRIC 226S
Advanced Optical Materials	Elucidating Orbital Delocalization Effects on Boosting Electrochemiluminescence Efficiency of Carbon Nitrides	FOTRIC 285
Advanced Materials	Geometric Phase and Localized Heat Diffusion	FOTRIC 347
Advanced Therapeutics	Regulation of ID4 In Vivo for Efficient Magnetothermal Therapy of Breast Cancer	FOTRIC 228S
ACS Nano	Graphene Oxide-Grafted Magnetic Nanorings Mediated Magnetothermodynamic Therapy Favoring Reactive Oxygen Species-Related Immune Response for Enhanced Antitumor Efficacy	FOTRIC 228S
ACS Nano	Ferrimagnetic Vortex Nanoring-Mediated Mild Magnetic Hyperthermia Imparts Potent Immunological Effect for Treating Cancer Metastasis	FOTRIC 228S
Nature	Brown-fat-mediated tumour suppression by cold-altered global metabolism	FOTRIC 285

Specifications

Model	229Pro	228Pro	226Pro
Thermal Imaging Parameters			
Infrared Resolution	1280 x 1024	640 x 480	384 x 288
Super Resolution(SR)	Support		
Detector Type	Uncooled FPA infrared detector		
Thermal Sensitivity (NETD)	30mk@30° C(86 °F)		40mk@30° C(86 °F)
Detector Pitch	12μm	17μm	17μm
Spectral Range	8~14μm		
Image Frame Rate	30Hz		
Field of View (FOV)	25° x 20°	25° x 19°	
Spatial Resolution (IFOV)	0.34mrad	0.68mrad	1.14mrad
Minimum Imaging Distance	0.4 m	0.25 m	0.1 m
Focal length	35mm	25mm	15mm
Focus Mode	TurboFocus™ system for continuous, laser-assisted, thermal contrast, and touch AF; Manual focus		
Lens Recognition	Automatic		
Optional Interchangeable Lens	46° Wide-angle Lens; 50μm Macro Lens	46° Wide-angle Lens; 20μm Macro Lens; 50μm Macro Lens	46° Wide-angle Lens; 50μm Macro Lens; 100μm Macro Lens
Digital Zoom	1-32x continuous zoom	1-16x continuous zoom	1-6x continuous zoom
Temperature Analysis			
Complete Temperature Range	-20~650°C (-4~1202 °F)		
Temperature Range	-20~120°C (-4~248 °F), 0~650°C (32~1202 °F), Intelligent range		
Temperature Extension	Support extension: lowest to -40°C / °F (Not applicable to macro lenses, measurement accuracy may exceed 2%), highest to 2000°C /3632 °F		
Accuracy	± 1°C /3.6 °F or ± 1 %, whichever is greater (ambient temp at 25°C /77 °F , temperature range 0° C-100° C/32 °F -212 °F), ± 2°C /3.6 °F or ± 2 % for other temperature range. Note: Macro lens can also achieve ±2°C /3.6 °F or ±2% measurement accuracy between -20° C(-4 °F)~400° C(752 °F)		± 2°C /3.6 °F or ± 2 %, whichever is greater (ambient temp at 25°C /77 °F). Note: Macro lens can also achieve ±2°C /3.6 °F or ±2% measurement accuracy between -20° C (-4 °F)~400° C(752 °F)
Measurement Tools	Spot: 18 Line: 6 Area: 18 AnalyzeIR: Unlimited ROIs	Spot: 15 Line: 6 Area: 15 AnalyzeIR: Unlimited ROIs	Spot: 9 Line: 3 Area: 9 AnalyzeIR: Unlimited ROIs

Specifications

Line Temperature Distribution	Support
Measurement Parameters	Emissivity, Reflected temperature, Ambient temperature, Humidity, Distance and IR window compensation.
Local Parameters	Support
Area Alarms	High temperature alarm and low temperature alarm
Temperature Rise Feature	Yes
On-Device Analysis	Support Radiometric Video and Image Analysis
PC Software	AnalyzIR Professional Analysis Software
Image Display	
Display Screen	5inch (landscape)1280 x 720 resolution
Image Mode	Thermal\Digital\Picture-in-Picture\T-DEF® Blend
Palette	16 standard + 16 inverted
Minimum Temperature Span	Auto (Minimum Temp Span 3°C), Manual (Minimum Temp Span 2°C), Touch-screen(Minimum Temp Span 2°C
Color Alarm	High temperature, low temperature, and interval isotherms
Hot and Cold Spot Tracing	Yes
Capture Features	
Digital Camera	2 Cameras: 5-mega pixel and 13-mega pixel
Storage Card	SD card of 256GB memory, support expansion to 2TB SD card of 128GB memory, support expansion to 2TB
Capture Mode	Single frame and Time-lapse
Image Format	JPEG(Radiometric), JPEG(Non-radiometric)
Video Format	IRS(Radiometric), MP4(Non-Radiometric)
Radiometric Video Recording	Support
Non-Radiometric Video Recording	Support
Gallery	Support viewing, editing and deleting image and video files
Remote Access	
PC	Remote Control Via AnalyzIR
Mobile Device	Through IRExplorer
Power System	
Battery Type	3.6V, 10000mAh lithium
Battery Life	Over 4 hours per battery
Battery Charging System	Battery charger, DC 13V charging, USB charging
Battery Charging Time	2.5 hours to 90% full charge
Energy Management	User-selectable screen-off modes

Specifications

Physical Parameters	
Operating Temperature	-20° C ~ 50° C(-4 °F ~122 °F)
Storage Temperature	-40° C ~ 70° C(-40 °F ~158 °F) without batteries
Language	
Languages	English, Spanish, French, German, Italian, Korean, Portuguese, Traditional Chinese, Thai
Configuration	
Packaging	Thermal imaging camera, lens, lens cap, 3 rechargeable lithium batteries, battery charger, power adapter, B5 R&D Bench, USB Type-C to USB interface cable, Micro HDMI interface to HDMI interface cable, SD card, SD card reader, accessory bag (wrist strap), information bag (packing list, calibration certificate, user manual), hard carrying case

FOTRIC

CONNECTING THE DIGITAL FUTURE

FOTRIC INC. All Rights reserved

Dec. 2024

www.FOTRIC.com